Deficiency of Starch Synthase IIIa and IVb Alters Starch Granule Morphology from Polyhedral to Spherical in Rice Endosperm[1]

Yoshiko Toyosawa[2], Yasushi Kawagoe[3], Ryo Matsushima, Naoko Crofts, Masahiro Ogawa, Masako Fukuda, Toshihiro Kumamaru, Yozo Okazaki, Miyako Kusano[4], Kazuki Saito, Kiminori Toyooka, Mayuko Sato, Yongfeng Ai, Jay-Lin Jane, Yasunori Nakamura, and Naoko Fujita*

Department of Biological Production, Akita Prefectural University, Akita City, Akita 010–0195, Japan (Y.T., N.C., Y.N., N.F.); Division of Plant Sciences, National Institute of Agrobiological Sciences, Tsukuba 305–8602, Japan (Y.K.); Institute of Plant Science and Resources, Okayama University, Kurashiki 710–0046, Japan (R.M.); Department of General Education, Yamaguchi Prefectural University, Yamaguchi 753–8502, Japan (M.O.); Plant Genetic Resources, Institute of Genetic Resources, Faculty of Agriculture, Kyushu University, Fukuoka 812–8581, Japan (M.F., T.K.); RIKEN Center for Sustainable Resource Science, Tsurumi-ku, Yokohama 230–0045, Japan (Y.O., M.K., K.S., K.T., M.S.); Graduate School of Pharmaceutical Sciences, Chiba University, Chuo-ku, Chiba 260–8675, Japan (K.S.); and Department of Food Science and Human Nutrition, Iowa State University, Ames, Iowa 50011–1120 (Y.A., J.-L.J.)

ORCID IDs: 0000-0002-6792-2232 (N.C.); 0000-0002-7570-2774 (J.-L.J.); 0000-0001-7660-0078 (Y.N.).

Starch granule morphology differs markedly among plant species. However, the mechanisms controlling starch granule morphology have not been elucidated. Rice (*Oryza sativa*) endosperm produces characteristic compound-type granules containing dozens of polyhedral starch granules within an amyloplast. Some other cereal species produce simple-type granules, in which only one starch granule is present per amyloplast. A double mutant rice deficient in the starch synthase (SS) genes *SSIIIa* and *SSIVb* (*ss3a ss4b*) produced spherical starch granules, whereas the parental single mutants produced polyhedral starch granules similar to the wild type. The *ss3a ss4b* amyloplasts contained compound-type starch granules during early developmental stages, and spherical granules were separated from each other during subsequent amyloplast development and seed dehydration. Analysis of glucan chain length distribution identified overlapping roles for SSIIIa and SSIVb in amylopectin chain synthesis, with a degree of polymerization of 42 or greater. Confocal fluorescence microscopy and immunoelectron microscopy of wild-type developing rice seeds revealed that the majority of SSIVb was localized between starch granules. Therefore, we propose that SSIIIa and SSIVb have crucial roles in determining starch granule morphology and in maintaining the amyloplast envelope structure. We present a model of spherical starch granule production.

Starch is the most important carbohydrate storage material and contains the Glc polymers amylose and amylopectin. At least four classes of enzymes, ADP-Glc pyrophosphorylase (AGPase), starch synthase (SS), starch branching enzyme (BE), and starch debranching enzyme (DBE), are necessary for efficient starch biosynthesis in storage tissues.

SSs (EC 2.4.1.21) play a central role in starch synthesis during α-glucan elongation by adding Glc residues from ADP-Glc to the nonreducing ends via α-1,4-glucosidic linkages. Rice (*Oryza sativa*) contains 11 SS genes that are grouped into six classes, SSI to SSV and granule-bound starch synthase (GBSS; Supplemental Fig. S1; Hirose and Terao, 2004; Ohdan et al., 2005). Every class contains multiple isozymes, except for SSI and SSV; SSI, SSIIa, SSIIIa, and GBSSI are highly expressed in developing rice endosperm (Hirose and Terao, 2004; Ohdan et al., 2005). SSI elongates short amylopectin chains with degree of polymerization (DP) from 6 or 7 to DP 8 to 12 (Fujita et al., 2006). SSIIa elongates amylopectin from DP 6 to 12 to DP 13 to 24 (Umemoto et al., 2002; Nakamura et al., 2005), and SSIIIa elongates long amylopectin chains with DP 33 or greater (Fujita et al., 2007). GBSSI synthesizes amylose and extra-long amylopectin chains (Sano, 1984; Takeda et al., 1987; Hizukuri, 1995). The functions of other SS isozymes, such as SSIIb, SSIIc, SSIIIb, SSIVa, SSIVb, SSV, and GBSSII, remain largely unknown due to the lack of respective mutant lines. It is not clear how SS isozymes contribute to starch granule formation.

Rice endosperm amyloplasts produce characteristic compound-type starch granules, which consist of dozens of polyhedral, sharp-edged granules (Matsushima et al., 2010). Compound-type starch granules are the most common type in endosperm of Poaceae species (Tateoka, 1962; Grass Phylogeny Working Group, 2001; Prasad et al., 2011; Matsushima et al., 2013). Simple-type starch granules (one starch granule per amyloplast) are produced in some species of the Bambusoideae, Pooideae, Micrairoideae, Chloridoideae, and Panicoideae subfamilies. The taxonomic relationships in the Poaceae do not enable an accurate prediction of granule morphology

(Tateoka 1962; Shapter et al., 2008; Matsushima et al., 2013).

Two studies that changed starch granule shape from simple type to compound type have been reported (Suh et al., 2004; Myers et al., 2011). A hull-less cultivar of cv Betzes barley (*Hordeum vulgare*), cv Nubet, contains simple-type and bimodal starch granules, which are typical of wild-type barley. Chemical mutagenesis of cv Nubet produced a mutant called *franubet*, which contains compound-type starch granules (Suh et al., 2004). In the maize monogalactosyldiacylglycerol synthase-deficient mutant *opaque5*, simple-type granules are replaced by compound-type granules separated by a membranous structure (Myers et al., 2011). The molecular mechanisms that control starch granule morphology in cereal endosperm are largely unknown, although an alteration in membrane lipid synthesis may be involved (Myers et al., 2011).

A structural model for the compound-type amyloplast is shown Figure 1. The amyloplast envelope contains an outer envelope membrane (OEM), inner envelope membrane (IEM), and intermembrane space (IMS). Each starch granule is enclosed by an IEM, and granules are separated by a septum-like structure (SLS; Yun and Kawagoe, 2010). In this model, the IMS and SLS are directly connected, and fluorescent proteins such as GFP and Cherry can move freely between the two (Fig. 1; Kawagoe, 2013). The chloroplast envelope membrane contains little protein compared with the thylakoid membrane (Heber and Heldt, 1981). The endosperm amyloplast envelope membrane contains even less protein. Low protein content could be a major reason why the amyloplast envelope in rice endosperm is difficult to observe using high-resolution electron microscopy. In transgenic rice, a fluorescent protein fused to an IEM protein, the ADP-Glc transporter BRITTLE1, visualized the amyloplast IEM (Yun and Kawagoe, 2010). Fluorescent proteins fused to the chloroplast OEM protein OEP7 visualized the amyloplast OEM in endosperm (Kawagoe, 2013). These studies revealed that the outermost membranes of rice amyloplasts are OEM and contain intraamyloplast compartments. Starch is synthesized within the amyloplast compartments and is ultimately formed as compound-type granules that are individually wrapped in IEM (Yun and Kawagoe, 2010; Kawagoe, 2013).

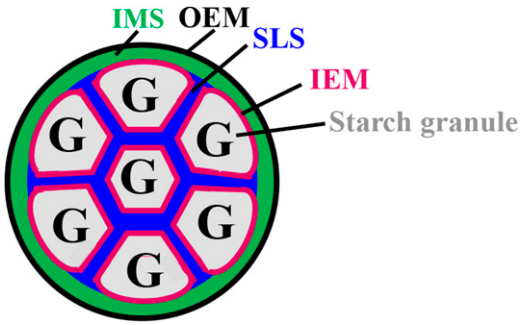

Figure 1. Structural model of the wild-type amyloplast in developing rice endosperm. The OEM is in black, the IEM is in magenta, the IMS is in green, and the SLS is in blue. G, Starch granules.

Confocal microscopy analyses of the rice IEM protein, BRITTLE1, revealed that an SLS, or cross wall, divides starch granules in the amyloplast (Yun and Kawagoe, 2010). A model for the synthesis of compound-type starch granules consisting of polyhedral, sharp-edged granules proposed that the SLS functions as a mold that casts growing granules into a characteristic shape (Yun and Kawagoe, 2010; Kawagoe, 2013). The model postulates a central role for the SLS in producing characteristic compound-type granules, although neither the SLS components nor the enzymes affecting its properties have been characterized.

Arabidopsis (*Arabidopsis thaliana*) SS genes are grouped into six classes. Leaf transitory starch biosynthesis has been investigated in single mutants of *SSI*, *SSII*, *SSIII*, and *SSIV* and in various double and triple SS mutants (Ral et al., 2004; Delvallé et al., 2005; Zhang et al., 2005, 2008; Szydlowski et al., 2009, 2011). Starch granules in leaf chloroplasts are reduced in number but enlarged in the *ssIV* mutant (Roldán et al., 2007; Crumpton-Taylor et al., 2013) and in the *ssIV* double and triple mutants (Szydlowski et al., 2009). Immature *ssIV* leaves have no starch granules but accumulate the starch synthase substrate ADP-Glc at high concentrations. Starch granules are flattened and discoid in wild-type leaves but are rounded in mature leaves of *ssIV*, suggesting that SSIV is essential for coordinating granule formation with chloroplast division during leaf expansion (Crumpton-Taylor et al., 2013). The *ssIII ssIV* double mutant does not accumulate measurable

[1] This work was supported by the Program for the Promotion of Basic and Applied Research for Innovations in Bio-oriented Industry (to N.F.) and the Science and Technology Research Promotion Program for Agriculture, Forestry, Fisheries, and Food Industry (grant no. 25033AB to N.F.).

[2] Present address: Plant Genetic Resources, Institute of Genetic Resources, Faculty of Agriculture, Kyushu University, Fukuoka 812–8581, Japan.

[3] Deceased.

[4] Present address: Graduate School of Life and Environmental Sciences, University of Tsukuba, 1-1-1 Tennodai, Tsukuba, Ibaraki 305–8572, Japan.

* Address correspondence to naokof@akita-pu.ac.jp.

The author responsible for distribution of materials integral to the findings presented in this article in accordance with the policy described in the Instructions for Authors (www.plantphysiol.org) is: Naoko Fujita (naokof@akita-pu.ac.jp).

Y.T. performed research, analyzed data, and wrote the article; Y.K. designed research, performed research, analyzed data, and wrote the article; R.M. performed research, analyzed data, and wrote the article; N.C. performed research and wrote the article; O.M. performed research, analyzed data, and wrote the article; M.F. performed research; T.K. performed research; Y.O. performed research and analyzed data; M.K. performed research; K.S. performed research; K.T. performed research; M.S. analyzed data; Y.A. analyzed data; J.-L.J. performed research; Y.N. performed research; N.F. designed research, performed research, analyzed data, and wrote the article.

www.plantphysiol.org/cgi/doi/10.1104/pp.15.01232

amounts of starch in the leaves, despite the presence of SSI and SSII activity (Szydlowski et al., 2009), implying that Arabidopsis SSIII and SSIV are involved in the initiation of starch granule formation and that either SSIII or SSIV is sufficient. Overexpression of *AtSSIV* increases the starch level in Arabidopsis leaves and potato (*Solanum tuberosum*) tubers (Gámez-Arjona et al., 2011). In transgenic plants, the AtSSIV-GFP fusion protein is enriched in specific regions at the edge of granules in Arabidopsis chloroplasts and potato tuber amyloplasts. In rice, *SSIVa* and *SSIVb* are expressed in the endosperm and other organs at an early developmental stage (Hirose and Terao, 2004; Ohdan et al., 2005).

In this study, two rice allelic SSIVb-deficient mutant lines (*ss4b*) were generated by insertion of the retrotransposon *Tos17* and crossed with the *SSIIIa* null mutant (*ss3a*). Surprisingly, the *ss3a ss4b* endosperm produced spherical starch granules that were separated from each other within amyloplasts, whereas the single mutants produced compound-type polyhedral starch granules. The SSIVb and GBSSI enzymes were localized to distinct compartments in developing amyloplasts. We discuss the changes in rice starch structure due to the deficiency of both SSIIIa and SSIVb, the alteration in starch granule morphology, and possible unconventional functions of SSIIIa and SSIVb. We also present a model of how spherical granules are produced in *ss3a ss4b* rice endosperm.

RESULTS

Isolation of *ss4b* and Production of *ss3a ss4b*

Two rice lines carrying *Tos17* within exon 8 (designated *e8*) or exon 14 (*e14*) of the *OsSSIVb* gene were identified (Supplemental Fig. S2). Seeds of *ss4b* mutants were translucent, whereas those of *ss3a* mutants had white cores (Fujita et al., 2007; Supplemental Fig. S3). In the crosses *ss3a* × *ss4b* (*e8*) and *ss3a* × *ss4b* (*e14*), segregation of translucent, white core, and opaque seeds fit the expected ratio of 12:3:1, with χ^2 values of 0.99 and 0.29, respectively ($P < 0.05$; Supplemental Table S1). Seedlings germinated from translucent seeds had the following genotypes: *SS3aSS3a SS4bSS4b*, *SS3ass3a SS4bSS4b*, *SS3aSS3a SS4bss4b*, *SS3ass3a SS4bss4b*, *SS3aSS3a ss4bss4b*, and *SS3ass3a ss4bss4b*. Seedlings germinated from white core seeds had the following genotypes: *ss3ass3a SS4bSS4b* and *ss3ass3a SS4bss4b*. All seedlings germinated from opaque seeds had the *ss3ass3a ss4bss4b* genotype. Consistent with these results, 100% of opaque seeds were produced only by plants that germinated from opaque seeds. Double homozygous mutant lines derived from *ss3a* × *ss4b* (*e8*), designated #*2012*, and *ss3a* × *ss4b* (*e14*), designated #*2013*, had similar phenotypes. Unless stated otherwise, the results for the *e8* (*ss4b*) and #*2012* (*ss3a ss4b*) lines are described.

Dehulled Grain Weight, Starch Quantity, and Lipid Composition in Mature Seeds

The grain weights of the wild-type (20.3 ± 0.3 mg), *ss3a* mutant (20.8 ± 0.2 mg), and *ss4b* mutant (21.2 ± 0.2 mg) rice were similar, whereas that of the *ss3a ss4b* double mutant was 86% of that of the wild type. The starch quantity in seeds of parental lines was 78.4% (*ss3a*) and 85.4% (*ss4b*) of the seed weight, which was similar to that of the wild type, whereas it was reduced to 56.9% in the *ss3a ss4b* double mutant (Table I).

The lipid contents of phosphatidyl choline, phosphatidyl ethanolamine, most of the triacylglycerol species, and some diacylglycerol species were higher in polished grains of *ss3a ss4b* than in polished grains of the wild type (pink-shaded cells in Supplemental Table S2) but lower in the bran of *ss3a ss4b* than in the bran of the wild type (blue-shaded cells in Supplemental Table S2; Supplemental Fig. S4). This indicates that the reduction in starch accumulation in the double mutant might lead to an increase in lipid accumulation in the endosperm (Kusano et al., 2012). The amounts of the 36:4, 36:5, and

Table I. *Characteristics of parental and mutant rice lines*

Dehulled grain weight, starch content, weight-average M_r, and *Z*-average radius of amylopectin gyration are shown for *ss3a ss4b* double mutant rice lines (*#2012* and *#2013*), the parental mutant lines *ss3a* (*e1*) and *ss4b* (*e8* and *e14*), and the wild-type rice, cv Nipponbare. Asterisks indicate significant differences between cv Nipponbare and mutant lines ($P < 0.05$, Student's *t* test). Dashes, Not analyzed.

Line	Genotype	Grain Weight[a]	Starch Content[b]	M_w[c]	R_z[d]
		mg		*×10⁸ g*	*nm*
cv Nipponbare	Wild type	20.3 ± 0.3 (100)	16.9 ± 1.2 (83.3)	43.7 ± 4.1 (100.0)	665.4 ± 26.9
e1	*ss3a*	20.8 ± 0.2 (102)	16.3 ± 1.1 (78.4)	10.4 ± 0.5* (23.8)	451.6 ± 8.9*
e8	*ss4b*	21.2 ± 0.2 (104)	18.1 ± 0.6 (85.4)	18.9 ± 1.4* (43.2)	474.9 ± 16.8*
e14	*ss4b*	17.8 ± 0.3* (85)[e]	12.2 ± 1.1 (68.5)	–	–
#2012	*ss3a ss4b*	17.4 ± 0.1* (86)	9.9 ± 0.4* (56.9)	5.1 ± 1.3* (11.7)	287.8 ± 9.2*
#2013	*ss3a ss4b*	16.6 ± 0.2* (81)	9.4 ± 1.0* (56.6)	–	–

[a]Values shown are means ± SE of 50 seeds, with percentages of the wild type given in parentheses. [b]Values shown are means ± SE of three seeds, with percentages of grain weight given in parentheses. [c]Weight-average M_r, with percentages of the wild type given in parentheses. [d]*Z*-average radius of gyration. [e]Note that the grain weights of *e14* (−/−) and *e14* (+/+), which were both segregated from the heterozygous parent *e14* (+/−), were 85% and 78%, respectively, of that of the wild type. This indicates that the reduction in grain weight in *e14*−/− did not result from the insertion of *Tos17* into the *SSIVb* gene.

36:3 digalactosyldiacylglycerol (DGDG) species, which are the main components of amyloplast membranes in maize endosperm (Myers et al., 2011), were unexpectedly very low in both polished grains and bran of *ss3a ss4b* (green-shaded cells in Supplemental Table S2). Instead, the amounts of 36:5 and 36:4 monogalactosyldiacylglycerol species and 34:1, 34:2, and 34:3 DGDG species, which are the minor components of amyloplast membranes in maize endosperm (Myers et al., 2011), were relatively high in rice and higher in polished grains of *ss3a ss4b* than in those of the wild type (green-shaded cells in Supplemental Table S2) but lower in the bran of *ss3a ss4b* than in the bran of the wild type (blue-shaded cells in Supplemental Table S2; Supplemental Fig. S4). A significant decline in the amount of monogalactosyldiacylglycerol and DGDG in the endosperm of the maize *opaque5* mutant, in which simple-type starch granules were replaced by compound-type starch granules, was reported by Myers et al. (2011). The relationship between the increase in polar lipid content in polished rice of *ss3a ss4b* and starch granule morphology is currently unknown.

Starch Granule Morphology in Mature Seeds

Mature wild-type and *ss4b* rice seeds cracked along the surface and within the amyloplasts to expose the inner polyhedral starch granules (Fig. 2A, a and c), whereas mature *ss3a* rice seeds tended to crack primarily along the amyloplast surface, possibly due to a substantial gap between the amyloplasts or physical weakness of the OEM (Fig. 2A, b and f). The inner starch granules were exposed in 5.9% of *ss3a* seeds, 38.1% of wild-type seeds, and 42% of *ss4b* seeds (Supplemental Table S3). The *ss3a ss4b* amyloplasts did not contain typical compound-type starch granules (Fig. 2Ad); the granules were spherical and were morphologically similar to maize simple-type starch granules (Jane et al., 1994). These observations were the same in both the central and peripheral endosperm of every line.

The contact points between wild-type amyloplasts were squashed flat and appeared to be covered by thick envelopes (Fig. 2Ae, arrows). By contrast, most *ss3a* amyloplasts had rounded surfaces with possible starch granule joints (Fig. 2Af, arrows). Putative envelope

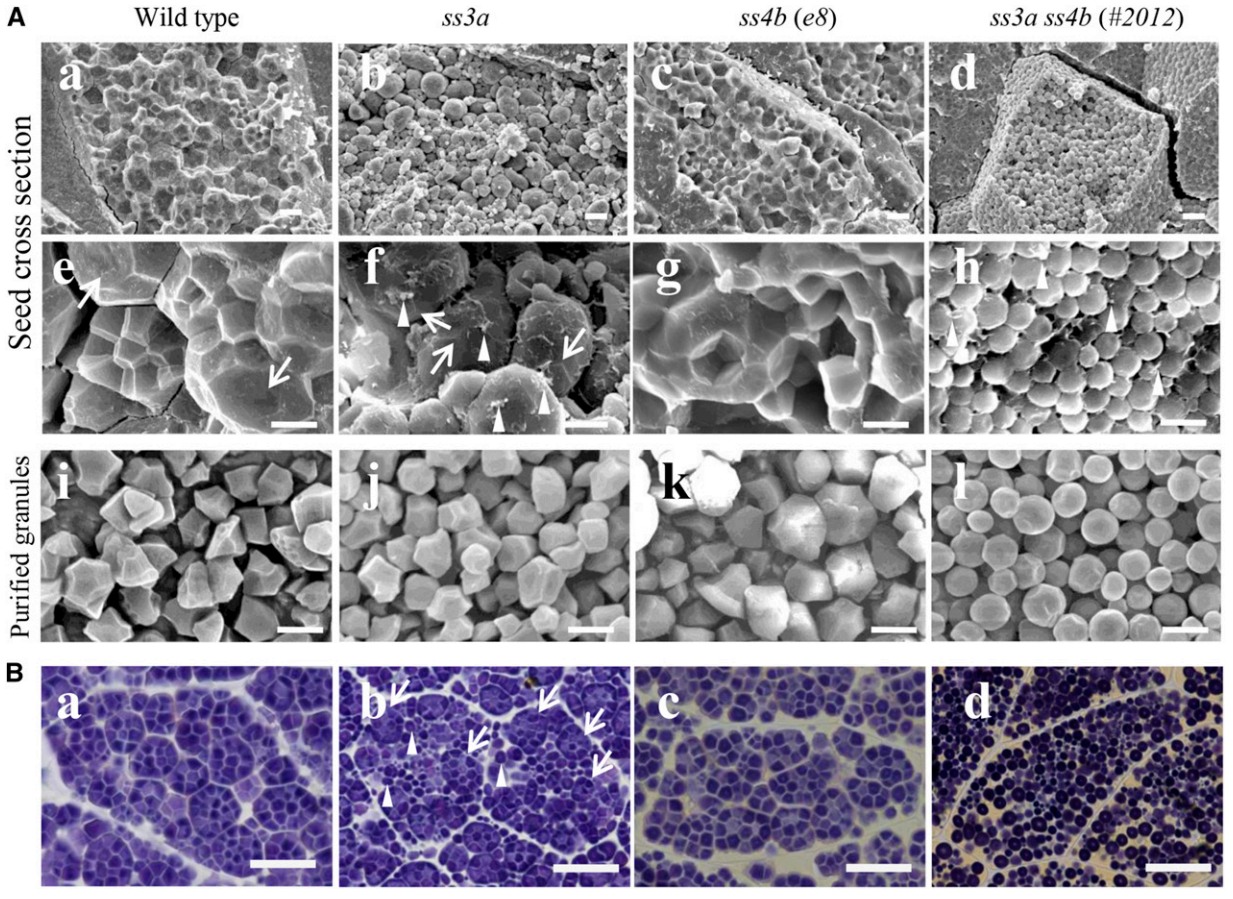

Figure 2. Starch granule morphology in mature rice seeds. A, Scanning electron micrographs of cross sections of mature seeds (central part of the endosperm; a–h) and purified starch granules (i–l). Arrows indicate the amyloplast surface, and arrowheads indicate putative shreds of the amyloplast envelope. Bars = 10 μm (a–d) and 5 μm (e–l). B, Light microscopy of iodine-stained thin cross sections of mature seeds (central part of the endosperm). Arrows indicate compound-type granules, and arrowheads indicate spherical granules. Bars = 20 μm.

shreds were detected on the starch granule surface of *ss3a* amyloplasts (Fig. 2Af, arrowheads). In *ss3a ss4b*, the spherical granules were not held together by the envelope (Fig. 2Ah; Supplemental Fig. S6A), and putative envelope shreds were detected on the surface of some, but not all, starch granules (Fig. 2Ah, arrowheads). We confirmed that purified starch granules were primarily spherical in *ss3a ss4b* but were primarily sharp edged and polyhedral in the wild type, *ss3a*, and *ss4b* (Fig. 2A, i–l; Supplemental Fig. S6A).

Iodine staining of the mature seed sections confirmed that spherical starch granules of the double mutant were well separated from each other, whereas typical compound-type starch granules were easily recognizable in the wild type and the two *ss4b* lines (Fig. 2B, a and c; Supplemental Fig. S6B). Two types of starch granules were observed in *ss3a*: spherical granules morphologically similar to those of *ss3a ss4b* (indicated by arrowheads in Fig. 2Bb) and typical compound-type starch granules (indicated by arrows in Fig. 2Bb) similar to those of the wild type and *ss4b*.

Morphology of Starch Granules and Amyloplasts in Developing Endosperm

To identify the developmental stages at which differences in starch granule morphology become apparent, we used light microscopy to examine thin iodine-stained sections of early developing endosperm cells (5−10 d after flowering [DAF]; Fig. 3). The starch granule size and starch content in endosperm cells of the single (*ss3a* and *ss4b*) and double (*ss3a ss4b*) mutants were less than those of the wild type at 7 and 10 DAF, indicating that starch accumulation and growth in the mutant lines are slower than in the wild type. Many typical amyloplasts containing polyhedral compound-type starch granules were observed in endosperm of single mutants and in the wild type. By contrast, the spherical starch granule shape of the double mutant became apparent at 7 DAF, and many starch granules assembled to form compound-like starch granule structures at 7 and 10 DAF (Fig. 3). The surface-localized starch granules in *ss3a* and the wild type were aligned to form a smooth amyloplast surface, whereas the surface of some *ss4b* amyloplasts appeared rough. Several spherical starch granules in *ss3a ss4b* were assembled, which made the amyloplast surface bumpy (Fig. 3).

Amyloplast and starch granule development was examined in developing wild-type and mutant seeds using transmission electron microscopy (TEM; Fig. 4A). Different amyloplast developmental stages were observed in subaleurone layer cells of wild-type seeds (Fig. 4A). Judging from the amyloplast sizes, the developmental stage of amyloplasts in Figure 4Ae corresponds to that of internal cells in the 5-DAF developing endosperm (Fig. 3A). Therefore, the developmental stages of the amyloplasts in Figure 4A, a to d, should be earlier. Empty amyloplasts, which were compartmentalized with membrane-like structures (Fig. 4Aa, center), and small nascent starch granules (Fig. 4Aa, right, small white particles) were observed. The starch granule sizes and the numbers of starch granules within amyloplast increased from Figure 4A, b to d. The mechanisms of

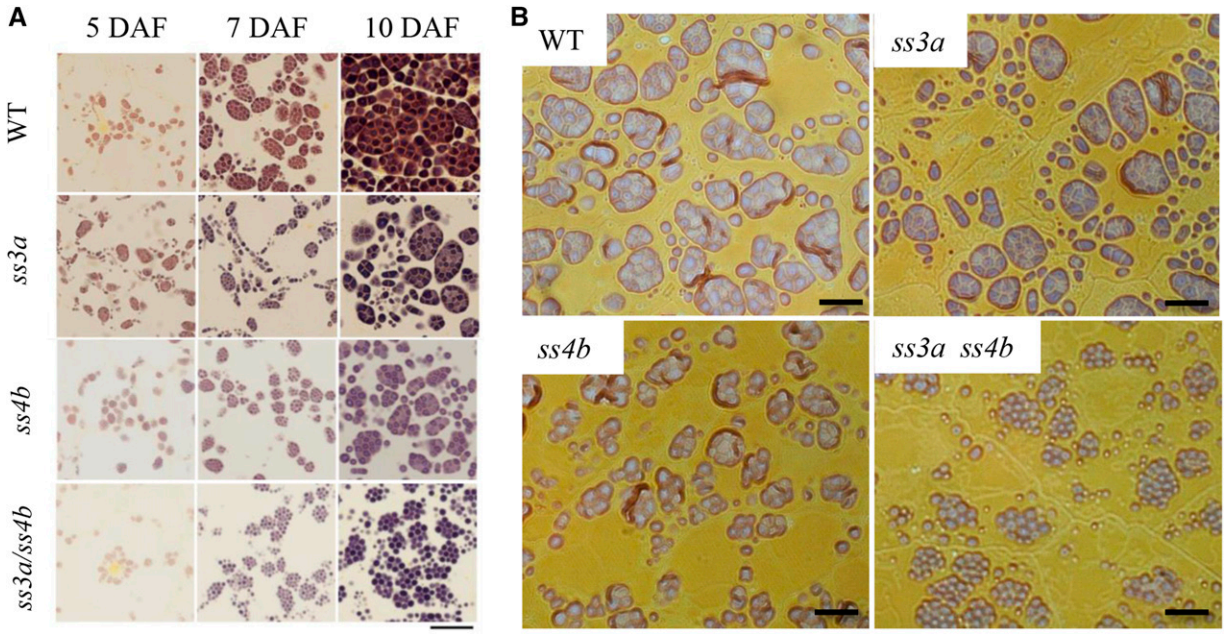

Figure 3. Starch granule morphology in developing endosperm. Light microscopy shows thin iodine-stained sections of the central part of the developing endosperm. Wild-type cv Nipponbare (WT), *ss3a*, *ss4b* (*e8*), and *ss3a ss4b* (*#2012*) were compared. A, Developing endosperm at 5, 7, and 10 DAF. Bar = 20 μm. B, Developing endosperm at 7 DAF. Bars = 10 μm.

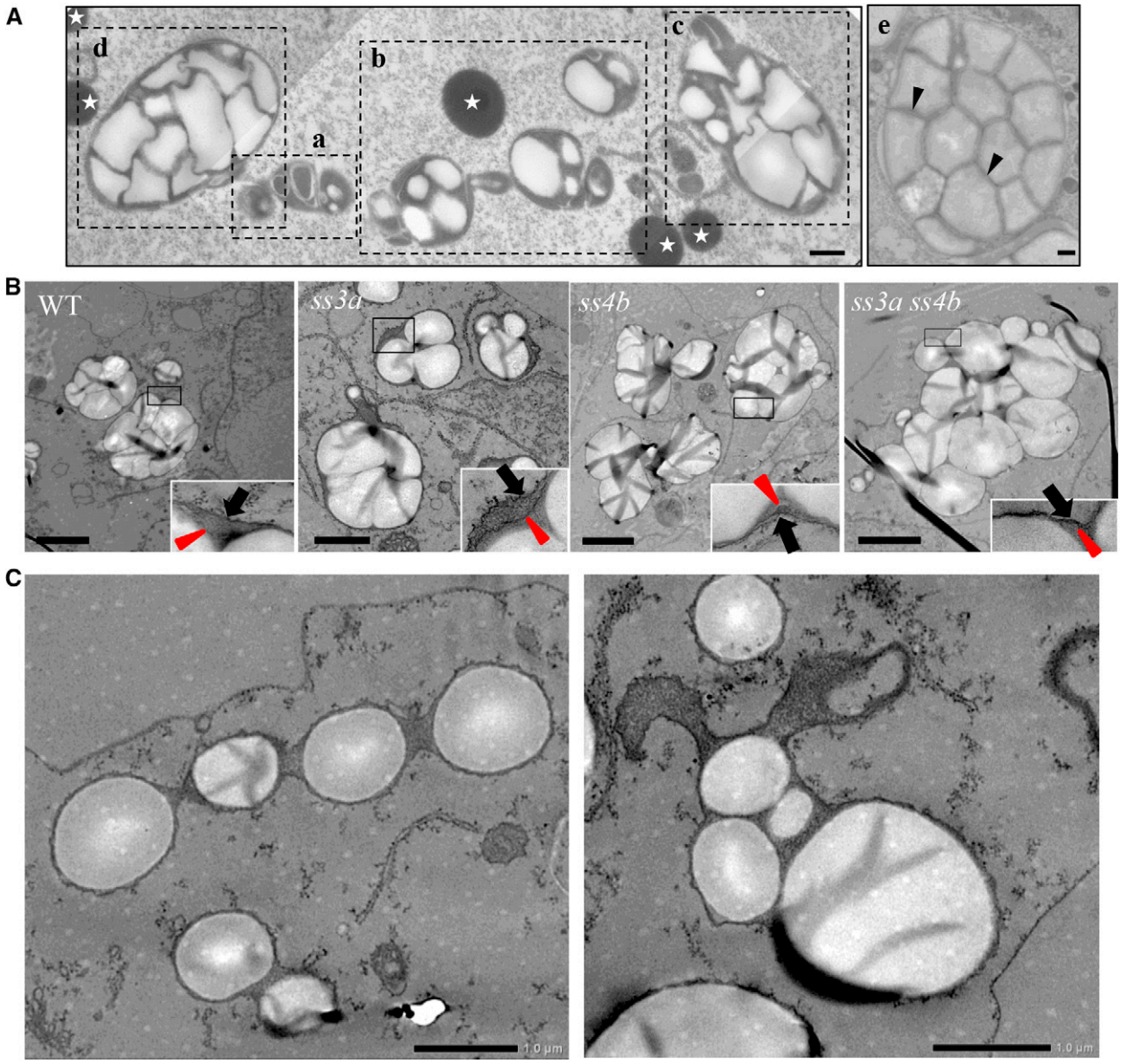

Figure 4. Transmission electron micrographs showing amyloplast morphology in developing rice starchy endosperm. A, Amyloplast development in the subaleurone layer cells of the wild type. a to e show amyloplasts at different developmental stages. Arrowheads indicate the IEM, and stars show protein bodies. Bars = 500 nm. B, Typical amyloplasts observed in ultrathin uranyl-lead-stained sections in the subaleurone layer cells at 7 DAF. Wild-type cv Nipponbare (WT), *ss3a*, *ss4b* (*e8*), and *ss3a ss4b* (*#2012*) were compared. Arrowheads indicate IEM, and arrows indicate outer amyloplast membrane. Bars = 2 μm. C, Aberrant *ss3a ss4b* amyloplasts in the subaleurone layer cells at 7 DAF. Bars = 1 μm.

amyloplast division occur as described by Yun and Kawagoe (2010). Even in wild-type seeds, starch granules were spherical (at least not polyhedral) at the early stages (Fig. 4A, a–c) before amyloplasts were filled with starch granules; enlarged IMS also was observed. Thereafter, IMS narrowed as starch granules grew (Fig. 4Ad). SLS lattices were pronounced and starch granules were wrapped with a thin envelope (IEM; arrowheads in Fig. 4Ae). Typical amyloplasts in subaleurone layer cells of 7-DAF mutant seeds were also observed by TEM (Fig. 4B; corresponding to the wild type in Fig. 4A, b and c). Multiple starch granules in *ss3a ss4b* and the wild type and parental mutant lines were wrapped with OEM, indicating that *ss3a ss4b* starch granules are initially produced as compound-type starch granules. The enlarged OEM images (Fig. 4B, insets) show that the surface-localized starch granules in *ss3a* and the wild type were all aligned to form a smooth amyloplast surface, whereas the surface of some *ss4b* and *ss3a ss4b* amyloplasts appeared rough (comparable with Fig. 3B). The frequency of amyloplasts displaying the pearl necklace-like structure was much higher in *ss3a ss4b*

(Fig. 4C, left) than in the wild type at a similar amyloplast developmental stage (Fig. 4A, a and b).

Localization of SS Isozymes

The amyloplast marker proteins tp^{GBSSI}GFP and tp^{GBSSI}Cherry, which contain the rice GBSSI transit peptide (Kawagoe, 2013), are efficiently targeted to the amyloplast stroma; however, it is not clear whether they are localized inside or outside the SLS. We generated transgenic rice plants that simultaneously express tp^{GBSSI}Cherry and GBSSI-GFP (full-length rice GBSSI N terminally fused to GFP). The fluorescent signals of the two markers did not overlap in amyloplasts. GBSSI-GFP was almost exclusively localized to starch granules in the amyloplast, except for the central area, whereas tp^{GBSSI}Cherry was detected in the spaces between starch granules (Fig. 5, A–C).

In transgenic rice plants expressing tp^{GBSSI}Cherry and SSIVb-GFP (full-length rice SSIVb N terminally fused to GFP), the GFP and Cherry signals showed considerable overlap (Fig. 5, D–F). In some amyloplasts, SSIVb-GFP was detectable as a bright focal point (Fig. 5E, arrowheads), as observed in Arabidopsis and potato expressing SSIV-GFP (Gámez-Arjona et al., 2011). The reason why SSIVb appears in this region as a punctate structure is unknown.

To visualize the internal amyloplast structures in mutant lines, we next generated rice plants expressing tp^{GBSSI}GFP in the endosperm. The developing amyloplasts of the mutant lines observed in Figure 6 corresponded to the wild-type stages observed in Figure 4A, b to d. In wild-type amyloplasts, GFP was almost exclusively localized to the area between starch granules, which is expected to correspond to the SLS (Kawagoe, 2013). The SLSs were observed as straight lines in optical thin sections in Z-series (Kawagoe, 2013), which indicates that SLSs extend as sheets that form a three-dimensional lattice within a spherical amyloplast. In *ss3a*, GFP was detected in the areas between starch granules and in an enlarged space at the amyloplast periphery (Fig. 6B, arrowheads). Many amyloplasts were irregularly shaped. In mature *ss4b* endosperm cells, the shapes of amyloplasts and granules were similar to those of the wild type (Fig. 2B), indicating that the amount of synthesized starch is sufficient to form starch granules as observed in the wild type. In the subaleurone layer of developing *ss4b* endosperm cells, most amyloplasts had SLS lattice structures similar to those of the wild type; however, some amyloplasts (less than 10% of total *ss4b* amyloplasts) did not have the clearly recognizable SLS structure (Fig. 6C). The amyloplast marked with an asterisk in Figure 6C appeared to contain starch granules but lacked a typical SLS lattice structure. Another representative *ss4b* amyloplast (dashed oval in Fig. 6C) contained a central cluster of small granules and large spherical granules at the periphery. These *ss4b* phenotypes were never observed in the wild type. As in *ss3a* (Fig. 6B), GFP was also detected in an enlarged space at the amyloplast periphery in *ss4b* (Fig. 6C, arrowheads). Most *ss3a ss4b* amyloplasts contained multiple spherical granules (Fig. 6D, arrowheads), whereas characteristic sharp-edged granules were rarely found. Residual amyloplasts seemed to produce simple-type starch granules with peripheral GFP signal (Fig. 6D, arrows).

To identify the subcellular localization of GBSS, SSIIIa, and SSIVb in outer endosperm cell amyloplasts of the 7-DAF wild type, immunoelectron microscopy was performed. Most GBSSI gold particles were detected at the periphery of the starch granules (Fig. 7, A and D; Supplemental Fig. S5, A–D). Most SSIIIa gold particles were detected on the starch granules, although some were detected at the OEM and IMS (Fig. 7, B and E). Many gold particles bound to SSIVb were detected between starch granules and, to a much lesser extent, on the starch granules (Fig. 7, C and F; Supplemental Fig. S5, I–L). The localization of each isozyme was distinct and consistent with those observed for GBSSI-GFP (Fig. 5B) and SSIVb-GFP (Fig. 5E), indicating that the labeling of the gold particles was likely to be specific.

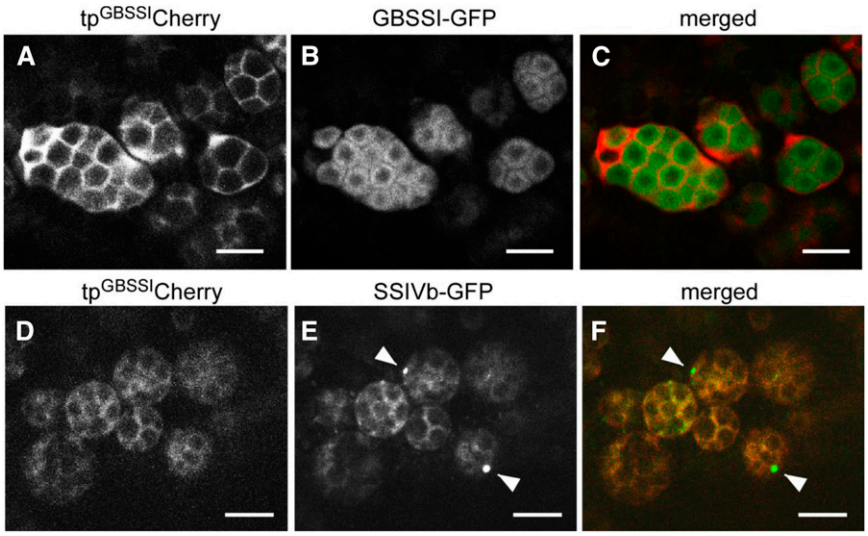

Figure 5. Distinct localizations of GBSSI and SSIVb. Confocal fluorescence microscopy shows developing seeds of transformed wild-type (cv Yukihikari) plants (7 DAF) expressing tp^{GBSSI}Cherry together with either GBSSI-GFP (A–C) or SSIVb-GFP (D–F). A to C, tp^{GBSSI}Cherry (magenta channel) and GBSSI-GFP (green channel). Note that the two signals do not overlap, indicating that tp^{GBSSI}Cherry is not efficiently imported into the stroma but is located primarily in the SLS and envelope. D to F, tp^{GBSSI}Cherry (magenta channel) and SSIVb-GFP (green channel). Note that the SSIVb-GFP and tp^{GBSSI}Cherry signals overlap extensively and that SSIVb-GFP is also detected as dots (arrowheads). Bars = 5 μm.

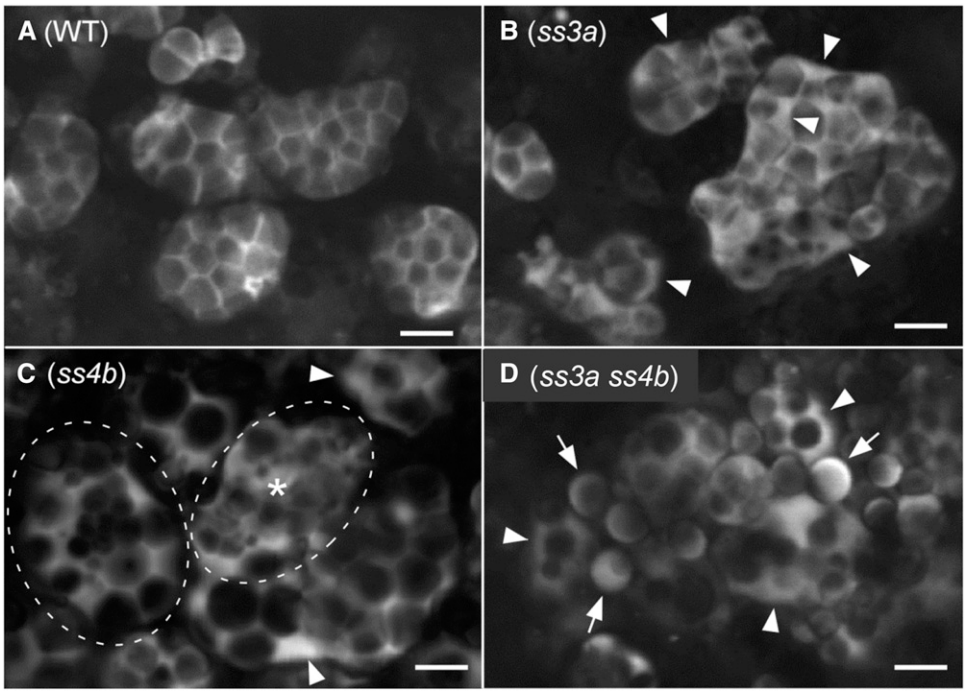

Figure 6. Internal structures of amyloplasts visualized with tp^{GBSSI}GFP. Developing seeds of the transformed wild-type (WT) cv Nipponbare (A), *ss3a* (B), *ss4b* (*e14*; C), and *ss3a ss4b* (*#2013*; D) were analyzed at 7 DAF by confocal microscopy. In B and C, arrowheads indicate enlarged IMS between the OEM and the IEM. In C, an amyloplast indicated by a dashed oval and asterisk does not contain a typical SLS lattice structure. Another amyloplast, indicated by a dashed oval, contains a cluster of small granules in the center and large granules at the periphery. Note that these distinct phenotypes in *ss4b* were observed with low frequency (less than 10%). Most amyloplast phenotypes were similar to that of the wild type. In D, arrowheads indicate amyloplasts containing multiple starch granules and arrows indicate granules that look like simple-type grains. Bars = 5 μm.

Analysis of Starch Structure

The fractionation of isoamylase-debranched starch from the wild type and mutants by size-exclusion chromatography resulted in three fractions (Fig. 8; Supplemental Table S4; Supplemental Fig. S6C). The λ_{max} values of the α-glucan-iodine complexes indicated that most, if not all, of the amylose, amylopectin long chains, and amylopectin short chains were contained in fraction I (eluted at approximately 150–200 min), fraction II (approximately 200–240 min), and fraction III (approximately 240–330 min), respectively. The apparent amylose content (AAC; the amount of fraction I from starch) was 22% in the wild type and 14.6% in *ss4b*. The AAC of *ss3a* was 30.8%, or 1.4 times that of the wild type, whereas the AAC of *ss3a ss4b* was 33.3% to 33.6%,

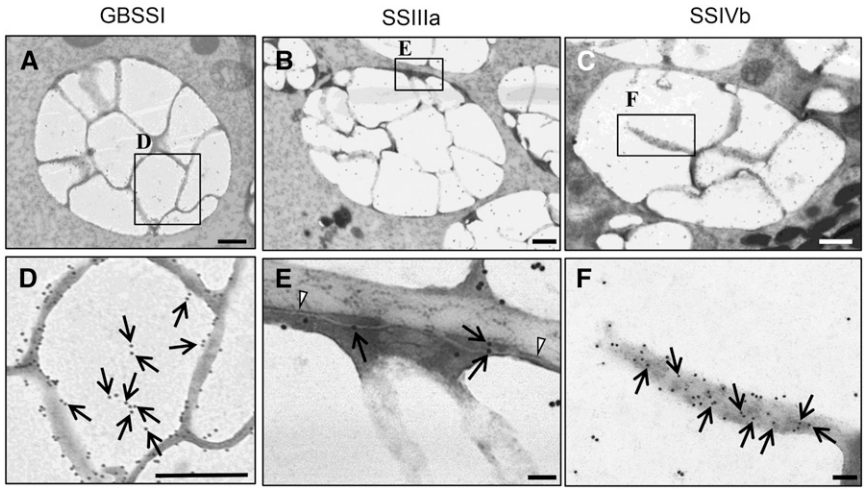

Figure 7. Immunoelectron microscopy of amyloplasts and the distribution of GBSSI, SSIIIa, and SSIVb in developing endosperm (7 DAF) of wild-type rice (cv Taichung 65). The distributions of GBSSI (A and D), SSIIIa (B and E), and SSIVb (C and F) are indicated by 15-nm gold particles (arrows). Arrowheads indicate the OEM. Bars = 500 nm (A–C) and 100 nm (D–F).

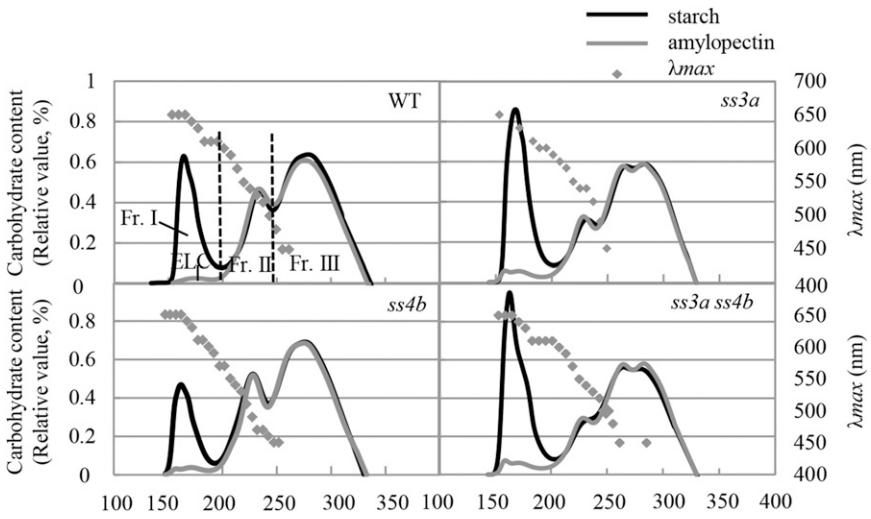

Figure 8. Gel filtration chromatography of isoamylase-debranched starch and purified amylopectin. Isoamylase-debranched starch (black lines) and purified amylopectin (gray lines) from wild-type cv Nipponbare (WT), *ss3a*, *ss4b* (*e8*), and *ss3a ss4b* (*#2012*) were analyzed by gel filtration chromatography on a series of Toyopearl HW55S and Toyopearl HW50S columns. The proportions of the starch components calculated from these data are shown in Supplemental Table S4. ELC, Extra-long chain; Fr., fraction.

or slightly (but significantly) higher than that of *ss3a*. The content of extra-long chains of amylopectin (also eluted in fraction I) was 1.4% in the wild type and *ss4b*, 2.9% in *ss3a*, and 2.9% to 3.8% in *ss3a ss4b* (Fig. 8; Supplemental Table S4; Supplemental Fig. S6C; Fujita et al., 2007). Fraction II primarily contained cluster-connecting chains (B_2 + B_3 and longer chains), whereas fraction III primarily represented short amylopectin chains within one cluster (A + B_1 chains; Hanashiro et al., 1996, 2011). The ratio of fraction III to fraction II in *ss4b* (3.1) was slightly higher than that in the wild type (2.6). This ratio was significantly higher in *ss3a* (4.5) and both *ss3a ss4b* lines (5) than in the wild type (Fig. 8; Supplemental Table S4; Supplemental Fig. S6C; Fujita et al., 2007).

Analysis of the chain length distribution in starch isoamylolysate using capillary electrophoresis revealed similarities between the wild type and *ss4b* (Fig. 9A; Supplemental Fig. S6D). In *ss3a* and *ss3a ss4b*, increases in DP 10 to 15 and DP 20 to 32 chains and reductions in DP 6 to 9, DP 16 to 19, and DP 33 or greater chains were observed (Fig. 9A; Supplemental Fig. S6D). These results for *ss3a* were consistent with those in our previous report (Fujita et al., 2007). Because the mol % of long chains was small, it was not easy to identify differences in long chains between samples; therefore, we calculated relative molar changes. The reduction in long-chain content (DP 35 or greater) was pronounced in both *ss3a* and *ss3a ss4b* (Fig. 9B; Supplemental Fig. S6E). The amounts of longer chains (DP 42 or greater) were lower in *ss3a ss4b* than in *ss3a*. Changes in the chain length distribution in *ss3a ss4b* seeds became apparent at 5 DAF (Supplemental Fig. S7).

The M_r of *ss3a* amylopectin was only 23.8% of that of the wild type (Table I), which is consistent with our previous report (Fujita et al., 2007). The M_r of amylopectinin *ss4b* and *ss3a ss4b* was 43.2% and 11.7%, respectively, of that of the wild type (Table I).

Analysis of starch granule crystallinity revealed typical A-type x-ray diffraction patterns in both the wild type and mutants (Supplemental Fig. S8). The height and sharpness of the major peaks in *ss4b* starch granules were nearly identical to those in the wild type. The major peaks in *ss3a* (approximately 70% of the wild type) and *ss3a ss4b* (approximately 80% of the wild type) starch granules indicated the lowest degree of crystallinity in *ss3a*.

SSIIIa and SSIVb Deficiency in the Mutant Lines Leads to Pleiotropic Effects on Other Enzymes

Native PAGE followed by SS activity staining did not detect SSIIIa activity in the *ss3a* and *ss3a ss4b* mutants (Fig. 10A). Immunoblot analyses with an antibody against rice SSIVb confirmed that SSIVb was present in developing seeds of the wild type and *ss3a* but not in those of *ss4b* or *ss3a ss4b* (Fig. 10B).

The activities and protein levels of other enzymes related to starch biosynthesis (SSI, phosphorylase1 [PHO1], DBEs [ISA1 or ISA1-ISA2 complex, ISA3, and PUL], and BEs) were similar in the wild type and mutants (Supplemental Figs. S9 and S10). In *ss3a ss4b*, the GBSSI protein level was 1.4 to 1.5 times that in the wild type (Supplemental Fig. S11A), and AGPase activity was 1.4 to 1.5 times that in the wild type and slightly higher than that in *ss3a* (Supplemental Fig. S11B). The level of SSIVa protein, but not that of SSIVb, increased in *ss3a* but was unchanged in *ss4b* (Supplemental Fig. S10).

We also compared the levels of proteins involved in amyloplast division (Yun and Kawagoe, 2009, 2010; Yun et al., 2011). The levels of FtsZ1 and FtsZ2-1 (components of the plastid division ring or Z-ring) increased only in *ss3a ss4b #2013* (Supplemental Fig. S10). By contrast, MinD and MinE (which control Z-ring formation at the division site) were present at similar levels in all lines (Supplemental Fig. S10). Given the similar levels of FtsZ and Min proteins in the wild type and *ss3a ss4b*, it is unlikely that spherical starch granules

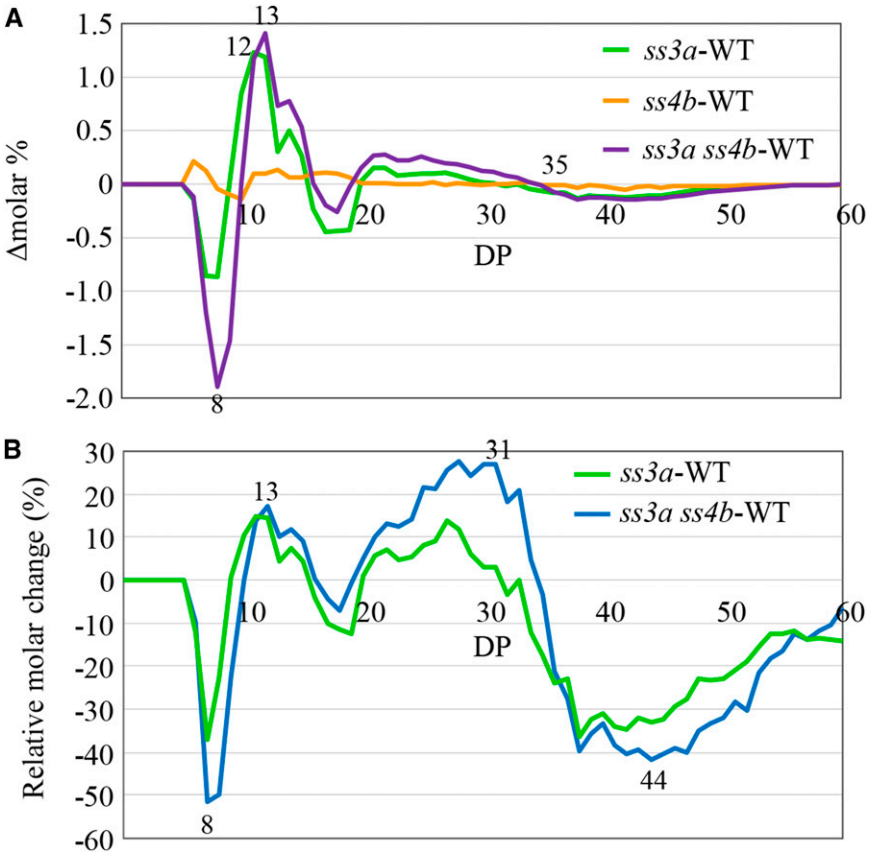

Figure 9. Chain length distribution patterns of amylopectin in wild-type rice and mutant lines. A, Differences in the chain length distribution patterns (Δmolar%) between mutant lines and wild-type cv Nipponbare (WT). Values represent averages of three seeds arbitrarily chosen from a single homozygous plant. B, Relative molar changes of each amylopectin chain (Δmol %/mol % × 100) calculated from the data shown in A for DP 6 to 60 for the wild type, *ss3a*, and *ss3a ss4b* (*#2012*). The numbers on the plots are DP values.

were produced in *ss3a ss4b* due to altered amyloplast division.

OsSSIVb Produced in *Escherichia coli* Has Starch Synthase Activity

SSIVb activity could not be detected in rice endosperm extracts (Fig. 10A). Therefore, we characterized recombinant full-length SSIVb and its catalytically inactive truncated version (as a negative control) produced in *E. coli* (Supplemental Fig. S12A). Full-length SSIVb was active only in the presence of amylopectin, and its activity was not significantly stimulated by citrate (Supplemental Fig. S12B). The SSIVb activity band contained protein(s) recognized by an anti-SSIVb antibody (Supplemental Fig. S12B).

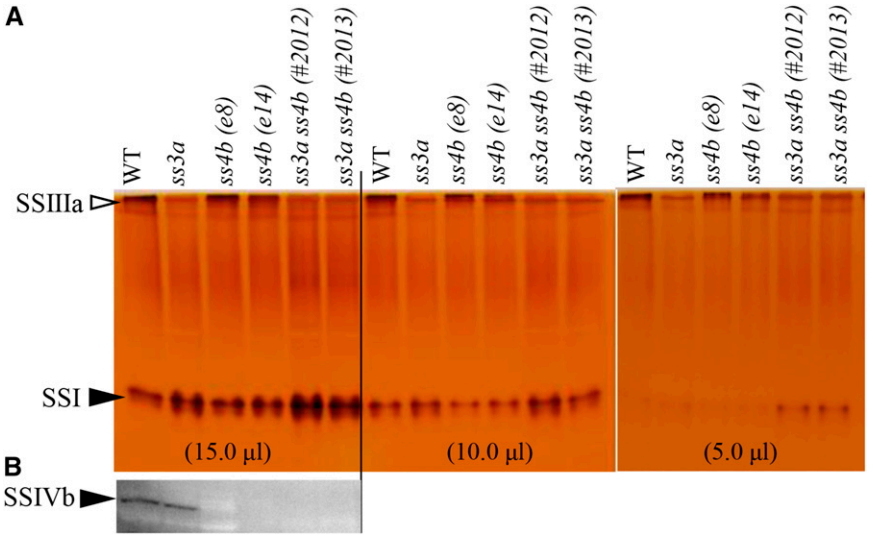

Figure 10. Detection of SS activity (SSI and SSIIIa) and SSIVb protein. Numbers in parentheses represent the volumes of the crude enzyme extract per lane. A, Native PAGE/SS activity staining. SSIIIa and SSI activity bands are indicated by arrowheads. B, Immunoblotting using antiserum against rice SSIVb. WT, Wild-type cv Nipponbare.

DISCUSSION

Possible Role of SSIIIa and SSIVb in the Initiation of Starch Synthesis

No changes in leaf starch structure are detected in an Arabidopsis SSIV-deficient mutant, although the number of starch granules per plastid is significantly lower and the granule size is larger than those of the wild type (Roldán et al., 2007). Seed morphology (Fig. 2; Supplemental Fig. S6) and amylopectin chain length distribution (Fig. 9; Supplemental Fig. S6D) in rice *ss4b* were similar to those in the wild type; however, AAC was lower than that in the wild type (Fig. 8; Supplemental Table S4; Supplemental Fig. S6C).

Starch granules are absent from the leaves of the Arabidopsis *ssIII ssIV* double mutant. Szydlowski et al. (2009) concluded that SSIV controls starch granule size, and starch granule initiation requires the presence of either SSIV or SSIII in Arabidopsis. In this study, we showed that rice mutants deficient in both SSIIIa and SSIVb accumulated a reduced, but still considerable, amount of endosperm starch. This strongly suggests that the initiation of starch granule synthesis in rice endosperm does not depend solely on SSIIIa and SSIVb. The M_r of amylopectin in *ss3a ss4b* endosperm was significantly lower than that in the wild type (Table I), and *ss3a ss4b* amylopectin contained fewer long chains with DP 42 or greater (connecting amylopectin clusters) than *ss3a* (Figs. 8 and 9; Supplemental Fig. S6, C–E). These results suggest that the functions of SSIIIa and SSIVb in long-chain amylopectin synthesis partially overlap.

Although the reason for differences in starch synthesis between Arabidopsis and rice double mutants is unclear, we found that the locations of SSIV in the respective plastids differ in the two species. In Arabidopsis leaf chloroplasts, SSIV-GFP was located primarily in specific regions at the boundaries of transitory starch granules (Szydlowski et al., 2009), whereas in rice endosperm amyloplasts, most, if not all, SSIVb was located between starch granules (as evidenced by fluorescence microscopy [Fig. 5, D–F] and immunogold labeling [Fig. 7B, b and d]). The two species also differ physiologically, in that starch is subjected to a daily synthesis/degradation cycle in Arabidopsis leaves whereas starch is synthesized and accumulated for long-term storage in rice endosperm. We believe that other rice isozymes expressed in developing endosperm, such as SSIIIb and SSIVa, may partly complement SSIIIa and SSIVb, although these expression levels are not high in the wild type (Ohdan et al., 2005). Although neither SSIVa nor SSIVb activity was detected in seed extracts (Fig. 10A), recombinant SSIVb synthesized glucans on native PAGE gels containing amylopectin (Supplemental Fig. S12B). Seed extracts show low expression of *SSIV*, which could explain why SSIV activity is undetectable, whereas strong *SSIV* expression is observed in sink leaves (Hirose and Terao, 2004; Ohdan et al., 2005). However, it is likely that the priming of starch granule synthesis does not require high expression of the crucial enzymes, because the number of starch granules per plastid is relatively low. The SSIII group is most closely related to the SSIV and SSV groups (Supplemental Fig. S1; Leterrier et al., 2008). Further studies of double and triple mutants with different knockout combinations among *ss3*, *ss4*, and *ss5* mutant lines are necessary to completely define the involvement of the corresponding SS isozymes in the initiation of starch granule synthesis in rice endosperm.

Previous reports and our starch structure data (Figs. 8 and 9; Supplemental Fig. S6, C–E) indicate that SSIIIa is the most abundant protein among SSIII and SSIV groups in rice endosperm, and it makes the major contribution to the elongation of long chains that connect between amylopectin clusters. The SSIVb expression level is the second highest among SSIII and SSIV groups in rice endosperm (Ohdan et al., 2005).

How Are Spherical Starch Granules Produced in *ss3a ss4b* Endosperm?

Starch granules in *ss3a ss4b* mature endosperm were primarily spherical and well separated from each other (Fig. 2; Supplemental Fig. S6A). They were morphologically similar to maize simple-type starch granules (Jane et al., 1994). Although spherical granules were observed at 7 DAF (Fig. 3A), most of them were still held together at that stage (Fig. 3). Many *ss3a ss4b* amyloplasts contained multiple granules within an amyloplast (Figs. 4B and 6D), indicating that *ss3a ss4b* starch granules were produced as compound-type starch granules.

During the early stages of wild-type starch development, before the amyloplast was filled with starch, granules had rounded corners and large IMS (Fig. 4A, a–d). These characteristics were similar to those in the mutant lines (Fig. 6, B–D). Subsequently, wild-type starch granules were enlarged together with the amyloplasts, and multiple amyloplasts were attached together. Finally, endosperm cells were filled with the polyhedral starch granules and amyloplasts (Fig. 2A, a and e). The rate of amyloplast development was much slower in the mutant lines than in the wild type (Fig. 3A). Therefore, spherical starch granules in *ss3a ss4b* including starch with lower M_r (Table I) are possibly due to the results from lower rates of starch biosynthesis and accumulation, and the significant reduction in long amylopectin chains, which connect amylopectin clusters and are important as backbones for building large amylopectin molecules. This could result in abundant empty spaces in and between amyloplasts after seed dehydration (Fig. 2, A and B). The phenotypic differences between *ss3a* (Fig. 2A, b and f) and *ss4b* (Fig. 2A, c and g) should result from differences in the contributions between SSIIIa and SSIVb to the elongation of amylopectin long chains (Figs. 8 and 9), as described in the previous section.

There are several rice mutant lines with reduced starch biosynthesis. For example, starch granules in

the shriveled seeds of a PHO1-deficient mutant line, in which starch biosynthesis is significantly repressed, have partially rounded corners and irregular shapes, whereas polyhedral starch granules accumulate in the plump seeds of a PHO1-deficient mutant (Satoh et al., 2008). The *ss1^L ss3a* double mutant rice line has extremely low SSI and other SS activities; more than half of the starch granules have rounded corners, the starch granule shapes are a mixture of oval, hemispherical, and irregular, and the starch granule sizes are random (Hayashi et al., 2015). By contrast, *ss3a ss4b* starch granules are qualitatively different from those of *pho1* (shriveled seeds) and *ss1^L ss3a*; all starch granules in *ss3a ss4b* were completely spherical with approximately equal sizes, and polyhedral starch granules did not occur. It appears that the amyloplast morphology in *ss3a ss4b* at 7 DAF, and probably even before 5 DAF, was quite different from that in the wild type (Fig. 3). These observations suggest that the production of spherical starch granules in *ss3a ss4b* cannot be completely explained by reductions in starch biosynthesis alone.

We compared the development of amyloplast morphology in the wild type and *ss3a ss4b* at the early stage of endosperm development using data from this study and previous reports (Supplemental Fig. S13). In the early endosperm of the wild type, typical dividing amyloplasts were elongated with multiple constrictions between starch granules (Supplemental Fig. S13A; Yun and Kawagoe, 2009). A subsequent increase in starch granule numbers in amyloplasts seemed to be due to successive SLS synthesis beneath the OEM; de novo starch granule synthesis occured in the stroma section divided by SLS and OEM (Supplemental Fig. S13B; Yun and Kawagoe, 2010). The new starch granules grow outward, with concomitant outgrowth of the OEM. ARC5 is recruited to the constriction sites from the cytosol (Yun and Kawagoe, 2009). The amyloplast division process involves septum constriction, OEM invagination, and separation of the new amyloplasts (Supplemental Fig. S13, C and D; Yun and Kawagoe, 2010). The numbers of starch granules and amyloplasts increase continuously until seed maturation. A proposed model for compound-type starch granule synthesis suggests that the SLS lattice separating starch granules and the envelope function together as a mold that casts growing granules into a characteristic polyhedral sharp-edged shape (Yun and Kawagoe, 2010; Kawagoe, 2013). As yet unknown components, SLS should be synthesized just after the stage of pearl necklace-like amyloplasts (Supplemental Fig. S13A) and is essential for amyloplast division and the formation of sharp-edged, compound-type starch granules (Kawagoe, 2013).

In the *ss3a ss4b* endosperm, pearl necklace-like amyloplasts were observed at an early stage (Fig. 4C, left). After the number of starch granules began to increase, multiple starch granules were coassembled (Figs. 3 and 4C, right; Supplemental Fig. S13, F–I), indicating that the mechanisms of the division process for increasing the number of starch granules in the double mutant were not compromised. The amyloplast surface in *ss3a ss4b* was bumpy (Fig. 4C, right; Supplemental Fig. S13, F–I). However, wild-type amyloplasts were spherical (Figs. 3 and 4; Supplemental Fig. S13, D–E).

These morphological differences between the wild type and *ss3a ss4b* at the stage of early developing endosperm might be caused by differences in SLS strength. SLS appears to function as the stretcher for making round amyloplast shape and as a mold for casting starch granules into polyhedral, sharp-edged shapes. The deficiency of SSIIIa and SSIVb might weaken the SLS, in that *ss3a ss4b* amyloplasts did not maintain a round shape. Starch granules that did not set into the mold grew freely and became spherical. The pearl necklace-like amyloplasts in *ss3a ss4b* (Fig. 4C, left) were observed with much higher frequency than in the wild type, suggesting that this amyloplast stage persisted for a longer period of time in *ss3a ss4b* than in the wild type (Supplemental Fig. S13, A–F). Starch granules in amyloplasts were readily divided in the wild type (Supplemental Fig. S13, A and B). These effects might be due to the vulnerable SLS or the significant reduction in starch biosynthesis in *ss3a ss4b*.

The reason why SSIIIa and SSIVb deficiency led to SLS instability is unknown. It is unknown whether both isozymes have a role in SLS formation or if only one of the two isozymes is involved. However, SSIVb was located on the SLS between starch granules (Figs. 5, D–F, and 7, C and F), and the *ss4b* amyloplast surface was bumpy (Fig. 3B), which suggests that SSIVb is important for SLS formation. By contrast, SSIIIa was located on the OEM and on starch granules (Fig. 7, B and E), and mature *ss3a* seeds had both substantial gaps between amyloplasts and OEM weakness (Fig. 2A, b and f), suggesting that SSIIIa is related to OEM formation. However, we could not confirm OEM weakness in developing endosperm of SSIIIa-deficient mutants by TEM (Fig. 4B).

We propose a model for amyloplast and starch granule formation in mutant lines and wild-type rice plants (Fig. 11) that is based on the hypothesis that only SSIVb is involved in SLS formation and is responsible for the significant reduction in starch biosynthesis in the double mutant (SSIIIa- and SSIVb-deficient) lines (Table I). Wild-type rice contains the robust SLS and amyloplast membranes, and the amyloplast maintains a round shape that is divided into multiple compartments by SLS (Fig. 11, developing stage, wild type). The starch granules are wrapped with IEM and grow in the stroma separated by the SLS mold. The starch granules and amyloplasts become enlarged and attach with neighboring amyloplasts until the seeds reach maturation. Therefore, the sharp-edged polyhedral starch granules in amyloplasts accumulate in wild-type endosperm cells (Fig. 11, mature stage, wild type).

The *ss3a* amyloplast maintained a round shape (Figs. 3 and 4), so the SLS should be normal. However, SSIIIa deficiency reduced starch biosynthesis in the endosperm during early seed development (Fig. 3A) because SSIIIa

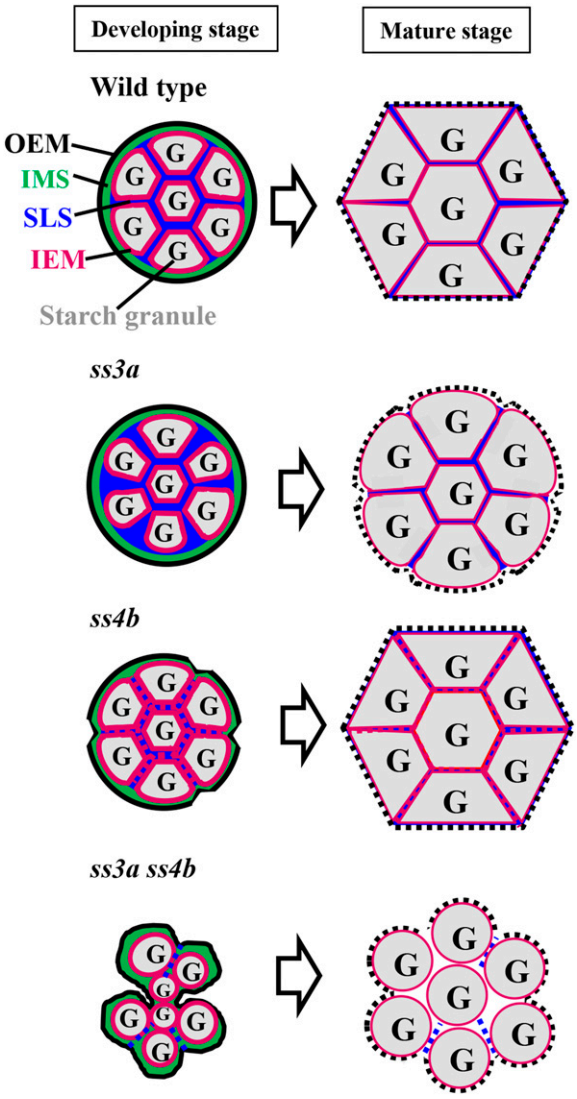

Figure 11. Possible molecular mechanism underlying amyloplast and starch granule synthesis in wild-type rice and mutant lines. Amyloplast development is shown in wild-type rice and in *ss3a*, *ss4b*, and *ss3a ss4b* mutants. At left are amyloplasts during early seed development (7 DAF), and at right are amyloplasts in mature seeds. The black dashed lines in mature seeds show the disrupted OEM during seed maturation and/or desiccation.

functioned to elongate long amylopectin chains (Figs. 8 and 9). The irregular starch granule shape and enlarged space at the *ss3a* amyloplast periphery in the tp^{GBSSI}GFP image (Fig. 6B) might be caused by a reduction in starch biosynthesis. Starch granules in the mature *ss3a* endosperm were loosely packed, there were many gaps between amyloplasts, and the starch granule periphery was rounded (Figs. 2Af and 11).

The surface of *ss4b* amyloplasts was bumpy because of their vulnerable SLS (Figs. 3B, 4B, and 11; Supplemental Fig. S13B). However, most amyloplasts were similar to those in the wild type, except for the bumpy outline (Fig. 3). Developing *ss4b* endosperm contained a cluster of small starch granules in the center of the cell, and large spherical granules were also observed at the periphery of the cell by the tp^{GBSSI}GFP image with low frequency (Fig. 6C). The function of SSIVb in amylopectin biosynthesis overlapped with that of SSIIIa (Fig. 9), although the contribution of SSIVb was much less than that of SSIIIa. SSIVb deficiency was compensated for by SSIIIa, indicating that the reduction in starch biosynthesis in *ss4b* was subtle (Table I). Therefore, the phenotype of mature *ss4b* endosperm was not significantly different from that of the wild type (Figs. 2A, c and g, and 11).

The *ss3a ss4b* amyloplast surface was also bumpy (Figs. 3B, 4, B and C, and 11; Supplemental Fig. S13B). Starch biosynthesis was reduced significantly due to the deficiency of both starch synthases that elongate amylopectin long chains (Table I). This resulted in larger spherical spaces in the developing *ss3a ss4b* endosperm (Fig. 6D) and a bumpier amyloplast surface than that of *ss4b* (Figs. 4B, 6D, and 11; Supplemental Fig. S13B). The *ss3a ss4b* starch granules did not set into the mold, and starch granules and amyloplasts were not attached to their neighbors. Therefore, the starch granules remained spherical until the seed reached maturity.

Further studies are needed to elucidate the components of the SLS and OEM that might be involved, and further detailed observations of amyloplast morphologies and membranes in developing endosperm of the mutant lines also are needed.

Unconventional Roles of SSIV Inferred from Phylogenetic and BLAST Analyses

A phylogenetic analysis by Deschamps et al. (2008) revealed that some glycogen synthases of some cyanobacteria and *Protochlamydia amoebophyla* (an obligate intracellular vertebrate pathogen) are classified into the SSIV group of higher plants. We conducted a similar phylogenetic analysis of starch synthases from higher plants (including rice and Arabidopsis) and a green alga (*Ostreococcus tauri*) as well as glycogen synthases from two cyanobacteria (*Synechocystis* sp. PCC 6803 and *Nostoc* sp. PCC 7120) and *P. amoebophyla*. The analysis confirmed that some, but not all, glycogen synthases of cyanobacteria and *P. amoebophyla* cluster with the SSIV group of higher plants (Supplemental Fig. S1; Supplemental Table S5). Ball et al. (2011) reported that the common ancestor of Archaeplastida, which contains Chloroplastida (green algae and land plants), Rhodophyceae (red algae), and Glaucophyta (glaucophytes), most likely possessed one gene for each SSIII-SSIV, SSI-SSII, and GBSSI. Bioinformatics analyses indicated that plants acquired the ancestral *SSIII-SSIV* gene by lateral gene transfer from *Protochlamydia* spp. (Moustafa et al., 2008; Ball et al., 2011).

We revealed that SSIIIa and SSIVb elongated long glucan chains equivalent to $B_{2\text{-}3}$ amylopectin chains

(Figs. 8 and 9; Supplemental Fig. S6D). Single mutants of $\Delta glgA_1$ (bacteria-type glycogen synthase) and $\Delta glgA_2$ (similar to higher plant SSIV) of *Synechocystis* sp. PCC 6803 accumulated glycogen, whereas the double mutant was unable to divide and was not viable after a few days of nitrate depletion (Gründel et al., 2012). The glycogen structure of $\Delta glgA_1$ was similar to that of the wild type, whereas that of $\Delta glgA_2$ contained more intermediate-length chains (DP 8−18) than the wild type (Yoo et al., 2014). Although the function of cyanobacterial $GlgA_2$ is still unknown, it is unlikely that this type of glycogen synthase synthesizes glucan chains comparable in length to the $B_{2\text{-}3}$ chains of amylopectin. This study suggested that at least SSIVb accounted for the physical strength of the SLS. Parallel studies on higher plant SSIVs and cyanobacterial glycogen synthases may shed new light on whether these ancient enzymes are essential for the formation of the SLS and amyloplast envelope as well as the cyanobacterial septum and cell wall.

A BLASTP search indicated that the SSIVb protein contains a region similar to several protein domains involved in chromosome segregation (SMC PROK domains). This suggests that SSIVb may be able to bind DNA. Reinhold et al. (2011) reported that β-amylase-like proteins are present in the nucleus rather than targeted to the chloroplast in Arabidopsis. SSIVb might act as a starch synthase and also as a DNA-binding protein such as a transcription factor. The noncatalytic region of SSIVb also contains the pfam01496 domain found in tonoplast ATPases. This may indicate that SSIVb can localize to the plastid membrane and tether the starch granules to the amyloplast membrane through physical interactions. Further analysis of SSIVb distribution outside the amyloplast and its relationships with other isozymes is needed.

MATERIALS AND METHODS

Plant Materials and Complementary DNA Clones

Rice (*Oryza sativa*) plants were grown during summer in an experimental paddy field under natural conditions. Two SSIVb-deficient mutant (*ss4b*) lines, *e8* and *e14*, containing *Tos17* insertions in exons 8 and 14 of the *OsSSIVb* gene, respectively, were obtained by *Tos17* mutagenesis (Supplemental Methods S1; Supplemental Fig. S2). The SSIIIa-deficient mutant (*ss3a*) line *e1*, containing a *Tos17* insertion in exon 1 of the *OsSSIIIa* gene, was described previously (Fujita et al., 2007). The parental *japonica* cv Nipponbare and cv Taichung 65 for TEM, and cv Yukihikari for transformation, were used as controls. To generate a double mutant deficient in SSIVb and SSIIIa (*ss3a ss4b*), we crossed *e8* and *e14* with *ss3a*, and the resulting double heterozygotes (F_1) were self-pollinated. Individual F_2 seeds segregated into three groups (translucent, white core, and opaque; Supplemental Table S1) according to their morphology. The segregation ratios were statistically examined using the χ^2 test (Supplemental Table S1). Full-length complementary DNA clones of *SSIVa* (AK100976), *SSIVb* (AK067577), and *GBSSI* (C19483) were obtained from the National Institute of Agrobiological Sciences.

Plasmid Construction, Rice Transformation, and Confocal Microscopy

The binary vectors used for *Agrobacterium tumefaciens*-mediated rice transformation were described previously (Onda et al., 2009; Yun and Kawagoe 2009, 2010). The transit peptide of rice GBSSI was translationally fused to the N terminus of the magenta fluorescent protein Cherry (Clontech) to yield tp^{GBSSI}Cherry, which is under the control of the rice *α-GLOBULIN* promoter and *GT1* terminator (Kawagoe et al., 2005). To construct the GBSSI-GFP fusion, the DNA fragment encoding M1-P609 of GBSSI was amplified by PCR using primers 5′-ATAGGTACCAACAGCTAGACAACCAC-3′ and 5′-GATCCAGGAGCAGCCACGTTCT-3′ and the EST clone C19483 as a template. To construct the SSIVb-GFP fusion, the DNA fragment encoding M1-A915 of SSIVb was amplified by PCR using primers 5′-ATAGGTACCCGCATCCGATTCCCAT-3′ and 5′-TATGGATCCTGCTGCTGCCCTCGCT-3′ and the EST clone AK067577 as a template.

Transformation of seed calli and plant regeneration were conducted as described previously (Kawagoe et al., 2005). Cross sections of transgenic rice seeds were analyzed as described previously (Yun and Kawagoe, 2009) using a TCS SP2 AOBS laser scanning confocal microscope (Leica Microsystems). The images were obtained at 488 and 543 nm and merged using Photoshop CS3 software (Adobe).

Light Microscopy

Thin Technovit sections were prepared according to Matsushima et al. (2010). Mature seed sections were prepared as follows: blocks (approximately 1 mm^3) were cut from the center of mature seed endosperm and fixed in a solution containing 5% (v/v) formalin, 5% (v/v) acetic acid, and 50% (v/v) ethanol for at least 12 h at room temperature. Samples were subsequently dehydrated in a graded ethanol series (30%, 50%, 70%, 90%, and 100% [v/v]) and embedded in Technovit 7100 resin (Kulzer). Thin sections (1 μm) were prepared using an ultramicrotome (Reichert-Nissei) and dried on coverslips.

Developing seed sections were prepared as follows: blocks (approximately 1 mm^3) were cut out from developing endosperm at 5, 7, and 10 DAF and fixed in 3% (v/v) glutaraldehyde in 20 mM cacodylate buffer (pH 7.4) for at least 24 h at 4°C. Samples were then dehydrated in a graded ethanol series (20%, 40%, 60%, 80%, and 100% [v/v]), embedded in Technovit 7100 resin, cut into 1-μm sections with an ultramicrotome (EM UC7; Leica Microsystems) and diamond knives, and dried on coverslips.

Sections were stained with Lugol solution (iodine:potassium iodine solution diluted in deionized water [1:40]; MP Biomedicals) for at least 5 s and examined with a microscope (AX70; Olympus).

Electron Microscopy

Mature seeds were cracked into halves with a knife. Scanning electron microscopy of these and purified starch granules was performed as described previously (Fujita et al., 2003, 2006, 2007). For TEM, sections of developing seeds were prepared as described by Takemoto et al. (2002). Thin pieces of developing seeds were sectioned in Murashige and Skoog medium containing 0.1% Suc. The samples were then placed in a specimen carrier containing the same medium supplemented with 0.1 M Suc and frozen in an EM-PACT high-pressure freezer (Leica). Samples were fixed in 0.5% glutaraldehyde in acetone at −80°C and embedded in LR White (London Resin). Thin sections (approximately 70 nm) were prepared using an ultramicrotome (Ultracut R; Leica) and subsequently immunolabeled as described by Toyooka et al. (2009).

Determination of Amylopectin M_r

The M_r of amylopectin was determined by HPSEC-MALLS-RI according to the methods of Yoo and Jane (2002) and Fujita et al. (2003).

Preparation of Starch Granules and Amylopectin for Gel Filtration

Starch granules were prepared from polished rice grains using the cold alkali method (Yamamoto et al., 1973, 1981). Amylopectin was isolated from starch granules using *n*-butanol according to Schoch (1954) as modified by Takeda et al. (1986). Starch and amylopectin were debranched with crystalline *Pseudomonas* spp. isoamylase (Hayashibara) according to Ikawa et al. (1981). Debranched materials were fractionated on a Toyopearl HW55S column (300 mm × 20 mm) connected in series to three Toyopearl HW50S columns (300 mm × 20 mm). The eluate refractive index was measured with an RI-8020 detector (Tosoh). Fractions I, II, and III were divided at the minimum values of the refractive index curves. The contents of apparent amylose, true amylose,

and extra-long chains in starch were calculated from the ratios of fractions I, II, and III. The contents of each fraction were confirmed by mixing the eluate with iodine and measuring the λ_{max} value with the spectrophotometer (Beckman Coulter) according to Horibata et al. (2004).

Chain Length Distribution of Endosperm Amylopectin

Starch was extracted from mature and developing rice endosperm according to Fujita et al. (2001). The chain length distribution of α-glucans was analyzed using the capillary electrophoresis method of O'Shea and Morell (1996) and Fujita et al. (2001) in a P/ACE MDQ Carbohydrate System (AB Sciex). Relative molar changes at each length were calculated by dividing the difference in mol % between samples by the mol % of each chain in the wild type.

Native PAGE, Activity Staining, and Enzyme Assays

Native PAGE was performed as described by Fujita et al. (1999). Staining for DBE and BE activity was performed according to the methods of Fujita et al. (1999) and Yamanouchi and Nakamura (1992), respectively. SS activity staining was performed on 7.5% (w/w) polyacrylamide gels containing 0.8% (w/v) oyster glycogen (Sigma) according to Nishi et al. (2001), except that 0.5 M citrate was included in the reaction mixture. PHO activity staining was performed on 5% (w/w) gels according to Satoh et al. (2008). The AGPase activity assay was performed according to Nakamura et al. (1989).

Sequence data from this article can be found in the GenBank/EMBL data libraries under accession numbers.

Supplemental Data

The following supplemental materials are available.

Supplemental Figure S1. Phylogenetic tree of starch synthases and glycogen synthases.

Supplemental Figure S2. Sites of *Tos17* insertion in the *OsSSIVb* gene and identification of the *Tos17* rice mutant lines by PCR.

Supplemental Figure S3. Morphological characterization of seeds from single and double mutants.

Supplemental Figure S4. Comparison of the total amounts of major lipids in bran and polished rice grain in *ss3a ss4b* and the wild type.

Supplemental Figure S5. Immunoelectron microscopy showing the distributions of SS isozymes.

Supplemental Figure S6. Starch traits in allelic mutant lines of *ss4b* and *ss3a ss4b*.

Supplemental Figure S7. Amylopectin chain length distribution pattern in developing endosperm of mutant lines.

Supplemental Figure S8. X-ray diffraction patterns of endosperm starch in wild-type cv Nipponbare and mutant lines.

Supplemental Figure S9. Native PAGE gel stained for starch biosynthesis enzyme activity in developing endosperm of wild-type cv Nipponbare and mutant lines.

Supplemental Figure S10. Immunoblot analyses with antibodies against SSIVb, SSIVa, FtsZ1, FtsZ2-1, MinD, MinE, and ISA3.

Supplemental Figure S11. Pleiotropic effects of SSIIIa and/or SSIVb deficiency on GBSSI protein levels and AGPase activity.

Supplemental Figure S12. Recombinant SSIVb exhibits starch synthase activity.

Supplemental Figure S13. Possible model of amyloplast development in early endosperm cells of the wild type and *ss3a ss4b*.

Supplemental Table S1. Segregation of F_2 seeds derived from a cross between *ss3a* and *ss4b* mutants according to normal, white core, and opaque morphologies.

Supplemental Table S2. Log_2 fold changes in the lipid profiles of bran and polished rice grains from wild-type cv Nipponbare and *ss3a ss4b #2012*.

Supplemental Table S3. Percentage of amyloplasts exposing inner starch granules when rice grains were cracked with a knife.

Supplemental Table S4. Composition of carbohydrate content in endosperm starch fractions separated by gel filtration chromatography.

Supplemental Table S5. Amino acid alignment used for phylogenetic analysis of starch synthases and glycogen synthases.

Supplemental Methods S1.

ACKNOWLEDGMENTS

We thank Dr. Hirohiko Hirochika and Dr. Akio Miyao (National Institute of Agrobiological Sciences Genome Resource Center) for providing the *Tos17* mutant panels, Naoko F. Oitome, Rumiko Itoh, Yuko Nakaizumi, and Mayumi Y. Goto (Akita Prefectural University) for technical support, Dr. Hiroaki Ichikawa (National Institute of Agrobiological Sciences Genome Resource Center) for summarizing the data of Dr. Yasushi Kawagoe, and Koji Takano, Makoto Kobayashi, and Atsushi Fukushima at the RIKEN Center for Sustainable Resource Science for technical assistance with lipid profiling and gas chromatography-mass spectrometry-based metabolite profiling.

Received August 6, 2015; accepted January 7, 2016; published January 8, 2016.

LITERATURE CITED

Ball S, Colleoni C, Cenci U, Raj JN, Tirtiaux C (2011) The evolution of glycogen and starch metabolism in eukaryotes gives molecular clues to understand the establishment of plastid endosymbiosis. J Exp Bot **62:** 1775–1801

Crumpton-Taylor M, Pike M, Lu KJ, Hylton CM, Feil R, Eicke S, Lunn JE, Zeeman SC, Smith AM (2013) Starch synthase 4 is essential for coordination of starch granule formation with chloroplast division during Arabidopsis leaf expansion. New Phytol **200:** 1064–1075

Delvallé D, Dumez S, Wattebled F, Roldán I, Planchot V, Berbezy P, Colonna P, Vyas D, Chatterjee M, Ball S, et al (2005) Soluble starch synthase I: a major determinant for the synthesis of amylopectin in *Arabidopsis thaliana* leaves. Plant J **43:** 398–412

Deschamps P, Colleoni C, Nakamura Y, Suzuki E, Putaux JL, Buléon A, Haebel S, Ritte G, Steup M, Falcón LI, et al (2008) Metabolic symbiosis and the birth of the plant kingdom. Mol Biol Evol **25:** 536–548

Fujita N, Hasegawa H, Taira T (2001) The isolation and characterization of a *waxy* mutant of diploid wheat (*Triticum monococcum* L.). Plant Sci **160:** 595–602

Fujita N, Kubo A, Francisco PB Jr, Nakakita M, Harada K, Minaka N, Nakamura Y (1999) Purification, characterization, and cDNA structure of isoamylase from developing endosperm of rice. Planta **208:** 283–293

Fujita N, Kubo A, Suh DS, Wong KS, Jane JL, Ozawa K, Takaiwa F, Inaba Y, Nakamura Y (2003) Antisense inhibition of isoamylase alters the structure of amylopectin and the physicochemical properties of starch in rice endosperm. Plant Cell Physiol **44:** 607–618

Fujita N, Yoshida M, Asakura N, Ohdan T, Miyao A, Hirochika H, Nakamura Y (2006) Function and characterization of starch synthase I using mutants in rice. Plant Physiol **140:** 1070–1084

Fujita N, Yoshida M, Kondo T, Saito K, Utsumi Y, Tokunaga T, Nishi A, Satoh H, Park JH, Jane JL, et al (2007) Characterization of SSIIIa-deficient mutants of rice: the function of SSIIIa and pleiotropic effects by SSIIIa deficiency in the rice endosperm. Plant Physiol **144:** 2009–2023

Gámez-Arjona FM, Li J, Raynaud S, Baroja-Fernández E, Muñoz FJ, Ovecka M, Ragel P, Bahaji A, Pozueta-Romero J, Mérida Á (2011) Enhancing the expression of starch synthase class IV results in increased levels of both transitory and long-term storage starch. Plant Biotechnol J **9:** 1049–1060

Grass Phylogeny Working Group (2001) Phylogeny and subfamilial classification of the grasses (Poaceae). Ann Mo Bot Gard **88:** 373–457

Gründel M, Scheunemann R, Lockau W, Zilliges Y (2012) Impaired glycogen synthesis causes metabolic overflow reactions and affects stress responses in the cyanobacterium *Synechocystis* sp. PCC 6803. Microbiology **158:** 3032–3043

Hanashiro I, Abe J, Hizukuri S (1996) A periodic distribution of the chain length of amylopectin as revealed by high-performance anion-exchange chromatography. Carbohydr Res **283:** 151–159

Hanashiro I, Higuchi T, Aihara S, Nakamura Y, Fujita N (2011) Structures of starches from rice mutants deficient in the starch synthase isozyme SSI or SSIIIa. Biomacromolecules **12:** 1621–1628

Hayashi M, Kodama M, Nakamura Y, Fujita N (2015) Thermal and Pasting Properties, Morphology of Starch Granules, and Crystallinity of Endosperm Starch in the Rice SSI and SSIIIa Double-Mutant. J Appl Glycosci **62:** 81–86

Heber U, Heldt HW (1981) The chloroplast envelope: structure, function, and role in leaf metabolism. Annu Rev Plant Physiol **32:** 139–168

Hirose T, Terao T (2004) A comprehensive expression analysis of the starch synthase gene family in rice (*Oryza sativa* L.). Planta **220:** 9–16

Hizukuri S (1995). Starch, analytical aspects. *In* AE Eliasson, ed, Carbohydrates in Food. Marcel Dekker, Lund, Sweden, pp 347–429

Horibata T, Nakamoto M, Fuwa H, Inouchi N (2004) Structural and physicochemical characteristics of endosperm starches of rice cultivars recently bred in Japan. J Appl Glycosci **51:** 303–313

Ikawa Y, Glover DV, Sugimoto Y, Fuwa H (1981) Some structural characteristics of starches of maize having a specific genetic background. Starke **33:** 9–13

Jane JL, Kasemsuwan T, Leas S, Zobel H, Robyt JF (1994) Anthology of starch granule morphology by scanning electron microscopy. Starke **46:** 121–129

Kawagoe Y (2013) The characteristic polyhedral, sharp-edged shape of compound-type starch granules in rice endosperm is achieved via the septum-like structure of the amyloplast. J Appl Glycosci **60:** 29–36

Kawagoe Y, Kubo A, Satoh H, Takaiwa F, Nakamura Y (2005) Roles of isoamylase and ADP-glucose pyrophosphorylase in starch granule synthesis in rice endosperm. Plant J **42:** 164–174

Kusano M, Fukushima A, Fujita N, Okazaki Y, Kobayashi M, Oitome NF, Ebana K, Saito K (2012) Deciphering starch quality of rice kernels using metabolite profiling and pedigree network analysis. Mol Plant **5:** 442–451

Leterrier M, Holappa LD, Broglie KE, Beckles DM (2008) Cloning, characterisation and comparative analysis of a starch synthase IV gene in wheat: functional and evolutionary implications. BMC Plant Biol **8:** 98

Matsushima R, Maekawa M, Fujita N, Sakamoto W (2010) A rapid, direct observation method to isolate mutants with defects in starch grain morphology in rice. Plant Cell Physiol **51:** 728–741

Matsushima R, Yamashita J, Kariyama S, Sakamoto W (2013) A phylogenetic re-evolution of morphological variations of starch grains among Poaceae species. J Appl Glycosci **53:** 37–44

Moustafa A, Reyes-Prieto A, Bhattacharya D (2008) Chlamydiae has contributed at least 55 genes to Plantae with predominantly plastid functions. PLoS ONE **3:** e2205

Myers AM, James MG, Lin Q, Yi G, Stinard PS, Hennen-Bierwagen TA, Becraft PW (2011) Maize *opaque5* encodes monogalactosyldiacylglycerol synthase and specifically affects galactolipids necessary for amyloplast and chloroplast function. Plant Cell **23:** 2331–2347

Nakamura Y, Francisco PB Jr, Hosaka Y, Sato A, Sawada T, Kubo A, Fujita N (2005) Essential amino acids of starch synthase IIa differentiate amylopectin structure and starch quality between *japonica* and *indica* rice varieties. Plant Mol Biol **58:** 213–227

Nakamura Y, Yuki K, Park SY, Ohya T (1989) Carbohydrate metabolism in the developing endosperm of rice grains. Plant Cell Physiol **30:** 833–839

Nishi A, Nakamura Y, Tanaka N, Satoh H (2001) Biochemical and genetic analysis of the effects of *amylose-extender* mutation in rice endosperm. Plant Physiol **127:** 459–472

Ohdan T, Francisco PB Jr, Sawada T, Hirose T, Terao T, Satoh H, Nakamura Y (2005) Expression profiling of genes involved in starch synthesis in sink and source organs of rice. J Exp Bot **56:** 3229–3244

Onda Y, Kumamaru T, Kawagoe Y (2009) ER membrane-localized oxidoreductase Ero1 is required for disulfide bond formation in the rice endosperm. Proc Natl Acad Sci USA **106:** 14156–14161

O'Shea MG, Morell MK (1996) High resolution slab gel electrophoresis of 8-amino-1,3,6-pyrenetrisulfonic acid (APTS) tagged oligosaccharides using a DNA sequencer. Electrophoresis **17:** 681–686

Prasad V, Strömberg CAE, Leaché AD, Samant B, Patnaik R, Tang L, Mohabey DM, Ge S, Sahni A (2011) Late Cretaceous origin of the rice tribe provides evidence for early diversification in Poaceae. Nat Commun **2:** 480

Ral JP, Derelle E, Ferraz C, Wattebled F, Farinas B, Corellou F, Buléon A, Slomianny MC, Delvalle D, d'Hulst C, et al (2004) Starch division and partitioning: a mechanism for granule propagation and maintenance in the picophytoplanktonic green alga *Ostreococcus tauri*. Plant Physiol **136:** 3333–3340

Reinhold H, Soyk S, Simková K, Hostettler C, Marafino J, Mainiero S, Vaughan CK, Monroe JD, Zeeman SC (2011) β-Amylase-like proteins function as transcription factors in *Arabidopsis*, controlling shoot growth and development. Plant Cell **23:** 1391–1403

Roldán I, Wattebled F, Lucas MM, Delvallé D, Planchot V, Jiménez S, Pérez R, Ball S, D'Hulst C, Mérida A (2007) The phenotype of soluble starch synthase IV defective mutants of *Arabidopsis thaliana* suggests a novel function of elongation enzymes in the control of starch granule formation. Plant J **49:** 492–504

Sano Y (1984) Differential regulation of waxy gene expression in rice endosperm. Theor Appl Genet **68:** 467–473

Satoh H, Shibahara K, Tokunaga T, Nishi A, Tasaki M, Hwang SK, Okita TW, Kaneko N, Fujita N, Yoshida M, et al (2008) Mutation of the plastidial α-glucan phosphorylase gene in rice affects the synthesis and structure of starch in the endosperm. Plant Cell **20:** 1833–1849

Schoch TJ (1954) Purification of the starch and the starch fractions. Methods Enzymol **3:** 5–6

Shapter F, Henry R, Lee L (2008) Endosperm and starch granule morphology in wild cereal relatives. Plant Genet Resour **6:** 85–97

Suh DS, Verhoeven T, Denyer K, Jane JL (2004) Characterization of Nubet and Franubet barley starches. Carbohydr Polym **56:** 85–93

Szydlowski N, Ragel P, Hennen-Bierwagen TA, Planchot V, Myers AM, Mérida A, d'Hulst C, Wattebled F (2011) Integrated functions among multiple starch synthases determine both amylopectin chain length and branch linkage location in *Arabidopsis* leaf starch. J Exp Bot **62:** 4547–4559

Szydlowski N, Ragel P, Raynaud S, Lucas MM, Roldán I, Montero M, Muñoz FJ, Ovecka M, Bahaji A, Planchot V, et al (2009) Starch granule initiation in *Arabidopsis* requires the presence of either class IV or class III starch synthases. Plant Cell **21:** 2443–2457

Takeda Y, Hizukuri S, Juliano BO (1986) Purification and structure of amylose from rice starch. Carbohydr Res **148:** 299–308

Takeda Y, Hizukuri S, Juliano BO (1987) Structures of rice amylopectins with low and high affinities for iodine. Carbohydr Res **168:** 79–88

Takemoto Y, Coughlan SJ, Okita TW, Satoh H, Ogawa M, Kumamaru T (2002) The rice mutant *esp2* greatly accumulates the glutelin precursor and deletes the protein disulfide isomerase. Plant Physiol **128:** 1212–1222

Tateoka T (1962) Starch grains of endosperm in grass systematics. Bot Mag Tokyo **75:** 377–383

Toyooka K, Goto Y, Asatsuma S, Koizumi M, Mitsui T, Matsuoka K (2009) A mobile secretory vesicle cluster involved in mass transport from the Golgi to the plant cell exterior. Plant Cell **21:** 1212–1229

Umemoto T, Yano M, Satoh H, Shomura A, Nakamura Y (2002) Mapping of a gene responsible for the difference in amylopectin structure between *japonica*-type and *indica*-type rice varieties. Theor Appl Genet **104:** 1–8

Yamamoto K, Sawada S, Onogaki I (1973) Properties of rice starch prepared by alkali method with various conditions. J Jpn Soc Starch Sci **20:** 99–104

Yamamoto K, Sawada S, Onogaki I (1981) Effects of quality and quantity of alkaline solution on the properties of the rice starch. J Jpn Soc Starch Sci **28:** 241–244

Yamanouchi H, Nakamura Y (1992) Organ specificity of isoforms of starch branching enzyme (Q-enzyme) in rice. Plant Cell Physiol **33:** 985–991

Yoo SH, Jane JL (2002) Molecular weights and gyration radii of amylopectins determined by high-performance size-exclusion chromatography equipped with multi-angle laser-light scattering and refractive index detectors. Carbohydr Polym **49:** 307–314

Yoo SH, Lee BH, Moon Y, Spalding MH, Jane JL (2014) Glycogen synthase isoforms in Synechocystis sp. PCC6803: identification of different roles to produce glycogen by targeted mutagenesis. PLoS ONE **9:** e91524

Yun MS, Kawagoe Y (2009) Amyloplast division progresses simultaneously at multiple sites in the endosperm of rice. Plant Cell Physiol **50:** 1617–1626

Yun MS, Kawagoe Y (2010) Septum formation in amyloplasts produces compound granules in the rice endosperm and is regulated by plastid division proteins. Plant Cell Physiol **51:** 1469–1479

Yun MS, Umemoto T, Kawagoe Y (2011) Rice debranching enzyme isoamylase3 facilitates starch metabolism and affects plastid morphogenesis. Plant Cell Physiol **52:** 1068–1082

Zhang X, Myers AM, James MG (2005) Mutations affecting starch synthase III in Arabidopsis alter leaf starch structure and increase the rate of starch synthesis. Plant Physiol **138:** 663–674

Zhang X, Szydlowski N, Delvallé D, D'Hulst C, James MG, Myers AM (2008) Overlapping functions of the starch synthases SSII and SSIII in amylopectin biosynthesis in *Arabidopsis*. BMC Plant Biol **8:** 96